

## Automatic Swing Control in Relaxation Oscillators

V8107 Mohammad Hossein Shakiba, Member, IEEE, and Tirdad Sowlati, Member, IEEE

XP-000880500

p. 1979-1986 = ①

p.d. 12-1998

E

**Abstract**—An automatic swing control (ASC) feedback is presented for relaxation voltage-controlled oscillators (VCO's). The ASC feedback maintains the oscillation swing at a constant level by dynamically adjusting the threshold voltage of the oscillator. The feedback mechanism provides a very wide linear frequency range and pushes saturation in the frequency characteristic of the oscillator to higher frequencies. As a result, operation close to the maximum achievable frequency, set by the inherent delay of the oscillation loop, becomes practically possible. Also, the sensitivity of the VCO frequency characteristic to process and temperature variations is reduced. These features make the ASC oscillator particularly suitable for autorate operation in serial-digital video applications. Detailed description of the design and experimental results of a trimmable VCO are given in this paper. It is shown that the frequency range is increased from 20–500 to 20–800 MHz when the ASC feedback is applied. In addition, statistical data from more than 1000 samples from several batches before and after trimming are provided. The results confirm the manufacturability of the ASC feedback approach. The implementations were done in a semicustom 14-GHz bipolar process.

**Index Terms**—Analog integrated circuits, bipolar transistor oscillators, oscillators, relaxation oscillators, voltage-controlled oscillators.

## I. INTRODUCTION

THE operation of a relaxation oscillator is based on alternately charging and discharging a capacitor by a reference current [1]. Relaxation-based voltage-controlled oscillators (VCO's) have been designed to operate up to several gigahertz [2]. Compared to ring and inductance-capacitance (LC)-tuned oscillators, they provide the widest tuning range and the best linear voltage-to-frequency characteristic. However, these oscillators usually suffer from poorer noise performance [3].

In a bipolar process, a relaxation oscillator can be realized as either an emitter- or a collector-coupled configuration [1], [4]. In the emitter-coupled configuration, sudden voltage jumps appear at both ends of the floating capacitor, where usually large parasitic capacitors to either substrate or ground are present. These jumps create excessive current spikes and possible substrate injection. On the other hand, the floating capacitor in a collector-coupled configuration does not experience sudden voltage jumps [4].

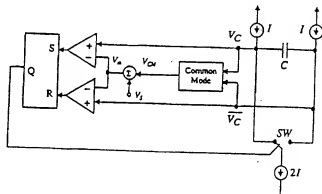


Fig. 1. A typical relaxation oscillator.

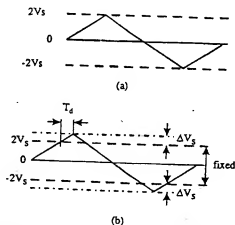


Fig. 2. Voltage waveform across the capacitor: (a) ideal case and (b) nonideal case.

Fig. 1 shows a simplified block diagram of a collector-coupled relaxation oscillator. For the switch position shown in this figure, the voltage at node  $\bar{V}_C$  increases linearly until it reaches the threshold level  $V_{th}$ . At this time, the latch is reset and the polarity of the current through the capacitor is reversed. The capacitor voltage starts to increase in the opposite direction until  $V_C$  reaches the threshold level. This sets the latch and completes one cycle of oscillation. As a result, the voltage across the capacitor swings with a peak amplitude of  $2V_S$ , where  $V_S = V_{th} - V_{CM}$  ( $V_{CM}$  is the common-mode voltage of  $V_C$  and  $\bar{V}_C$ ). In practice,  $V_{CM}$  is set to a reference value in a common-mode feedback loop, not shown in Fig. 1 for simplicity. The capacitor voltage waveform is illustrated in Fig. 2(a). In the ideal case, the frequency of oscillation is linearly dependent on the current and inversely proportional to the capacitance and its voltage

Manuscript received April 17, 1998; revised July 14, 1998.

M. H. Shakiba is with Gennum Corp., Burlington, Ont. L7L 5P5 Canada (e-mail: hosai@gennum.com).

T. Sowlati is with Gennum Corp., Burlington, Ont. L7L 5P5 Canada. He is now with Phillips Research, Briar Cliff Manor, NY 10510 USA. Publisher Item Identifier S 0018-9200(98)08859-3.

<sup>1</sup>The controlling parameter is a current rather than a voltage, and usually a voltage-to-current converter is used.

swing

$$f = \frac{I}{8CV_S} \quad (1)$$

To derive this formula, it is assumed that as soon as  $V_C$  or  $\bar{V}_C$  reaches  $V_{th}$ , the switch toggles instantly. However, there is a delay associated with the comparator, the set-reset (SR) latch, and the switch. During this delay  $T_d$ , the voltage across the capacitor continues to rise or fall in the same direction by the amount  $\Delta V_S = IT_d/C$ , as shown in Fig. 2(b). As a result, the voltage swing across the capacitor is no longer fixed, and the actual amplitude of the capacitor voltage swing becomes

$$V_{S,act}(I) = 2V_S + \frac{IT_d}{C} \quad (2)$$

The above change in the capacitor swing can be viewed as an increase in the threshold voltage, making it a function of the charging current

$$V_{th,act}(I) = V_{CM} + V_S + \frac{IT_d}{2C} \quad (3)$$

As a result, the frequency of oscillation drops to

$$f = \frac{I}{4CV_{S,act}} = \frac{1}{8CV_S + 4T_d I} \quad (4)$$

As (4) shows, the linear relationship between current and frequency is approximate. At low frequencies,  $T_d$  can be ignored and linearity is good. At high frequencies,  $T_d$  is comparable with the period of oscillations, and consequently, the  $I$ - $F$  characteristic becomes nonlinear. Also, when  $I$  is increased, the frequency slowly approaches its maximum limit of

$$f_{lim} = \frac{1}{4T_d} \quad (5)$$

However, operation of the oscillator close to  $f_{lim}$  is practically impossible because of the excessive current requirement. Furthermore, since the capacitor voltage swing increases with  $I$ , the circuit should be designed to handle a much larger voltage swing. As the delay  $T_d$  is dependent on temperature and process, the sensitivity of the oscillator to these factors increases as the frequency increases. For autotune operation in serial-digital video applications [5], where operation at multiple center frequencies is required, it is desired to design the VCO such that its voltage-to-frequency characteristic is insensitive to process and temperature variations over a wide frequency range. The presence of  $T_d$  in (4) indicates that this goal cannot be achieved by trimming the VCO at one frequency. In the following section, a feedback control over the oscillator threshold voltage will be introduced to overcome the aforementioned limitations.

## II. THE AUTOMATIC SWING CONTROL CONCEPT

The basic idea in ASC feedback is to replace the fixed swing voltage,  $V_S$  in Fig. 1, with a variable voltage [6]. This

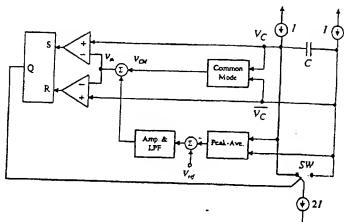


Fig. 3. ASC relaxation oscillator.

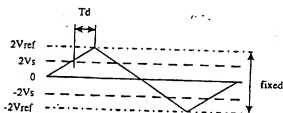


Fig. 4. Voltage waveform across the capacitor in the ASC VCO.

voltage is adaptively adjusted to compensate for the threshold increase described by (3). Fig. 3 shows the block diagram of a relaxation VCO that incorporates the ASC feedback loop. Here, the desired voltage swing of the capacitor is applied to the oscillator as the reference voltage of the control loop  $V_{ref}$ . The capacitor voltage swing is extracted by subtracting the average voltage of  $V_C$  and  $\bar{V}_C$  from their peak value. The extracted swing is compared with the reference voltage to generate an error signal, which is then amplified and low-pass filtered. The resulting signal, when added to the common-mode voltage  $V_{CM}$ , provides the oscillator with a threshold level that could vary between  $V_{CM}$  and  $V_{CM} + V_{ref}$ . By having a large dc gain in the ASC feedback loop, the threshold voltage settles at a level that forces the error signal to almost zero. As shown in Fig. 4, the voltage swing across the capacitor becomes independent of the charging current and has a constant peak amplitude of  $2V_{ref}$ . The frequency becomes a linear function of the current even at high frequencies

$$f = \frac{I}{8CV_{ref}} \quad \text{for } f < f_{lim} \quad (6)$$

where  $f_{lim}$  is set by the process and is given by (5). Furthermore, operation close to this frequency is achievable in practice because the feedback loop can force  $V_S$  to zero. Also, note that high-frequency operation of the ASC VCO does not require the excessive current that is predicted by (4) for a conventional relaxation VCO. Fig. 5 is a typical illustration of the frequency and voltage swing characteristics of the conventional and ASC relaxation VCO's shown in Figs. 1 and 3. Note that for the ASC oscillator, the swing is kept constant up to the point where the feedback loop has decreased  $V_S$

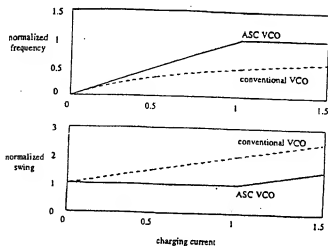


Fig. 5. Frequency and swing characteristics of the conventional and ASC relaxation VCO's (frequency is normalized to its maximum and swing to its minimum).

down to zero. At this point, the frequency has reached its limit and cannot be increased beyond that.

### III. CIRCUIT DESCRIPTION

#### A. Relaxation VCO

Fig. 6 shows the circuit diagram of the collector-coupled relaxation VCO. In accordance with Fig. 1, this circuit was designed and fabricated as our reference for evaluating the performance of the VCO after the ASC loop was added. Here, transistors  $Q_1$  and  $Q_2$  form the switch SW and direct current  $I_C$  to charge and discharge capacitor  $C_1$ . Pullup resistors  $R_1$  and  $R_2$  are used instead of current sources to eliminate the need for a common-mode feedback and PNP or PMOS transistors. The available PNP transistors in our process have a low early voltage, high parasitic capacitances, and low beta. To achieve a reasonable beta, many PNP transistors are required. This increases the parasitics to a value close to  $C_1$ . In addition, a beta-compensation circuit for PNP transistors is required to handle the wide variations in  $I_C$ .  $Q_3$ ,  $Q_4$ , and  $R_3$  in Fig. 6 act as a negative resistance to compensate for the current variations in the pullup resistors due to the voltage swing across them [7]. As a result, capacitor  $C_1$  is charged and discharged with a constant current. It should be mentioned that in this approach, the common-mode voltage  $V_{CM}$  is a function of  $I_C$ . The variation in  $V_{CM}$  results in a change in the junction capacitances at nodes  $V_C$  and  $\bar{V}_C$ . However, these changes are small compared to  $C_1$  and have a negligible effect on the frequency of oscillation.  $R_6$ ,  $R_7$ , and  $C_2$  extract the common-mode voltage of the capacitor terminals. This voltage is buffered by  $Q_9$  and serves as the threshold voltage of the SR latch. The latch consists of  $Q_5$ ,  $Q_6$ ,  $R_4$ , and  $R_5$ . Assuming  $Q_5$  is on and  $Q_6$  is off, the voltage at the base of  $Q_7$  is compared with that of  $Q_3$ , which is effectively the miter voltage of  $Q_9$ . As soon as this voltage passes the threshold level,  $Q_7$  starts to conduct and, through the positive feedback of the latch, turns off  $Q_3$  and turns on  $Q_8$ . This changes the state of the latch, and consequently the state of

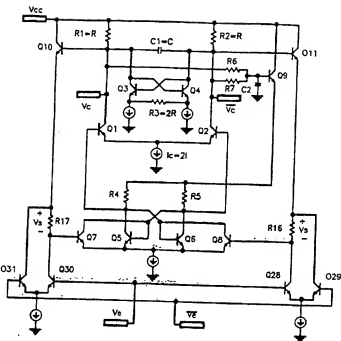


Fig. 6. Circuit diagram of the conventional relaxation oscillator.

the switch, and reverses the direction of the current through  $C_1$ .

The mechanism through which the swing amplitude is set is slightly different from (but equivalent to) what was shown in Fig. 1. Rather than being added to the common-mode voltage, the reference voltage is subtracted from both  $V_C$  and  $\bar{V}_C$  through dc voltage drops across resistors  $R_{17}$  and  $R_{16}$ . Transistors  $Q_{10}$  and  $Q_{11}$  buffer  $V_C$  and  $\bar{V}_C$  before level shifting. These transistors also compensate for the  $V_{BE}$  drop of  $Q_9$ , which is used to buffer  $V_{CM}$ . For best compensation, the currents of these three transistors should be equal. DC-level-shifted versions of  $V_C$  and  $\bar{V}_C$  are fed to the bases of  $Q_7$  and  $Q_8$  to toggle the state of the latch.

The differential voltage applied to  $V_C$  and  $\bar{V}_C$  controls the amount of the current through  $R_{16}$  and  $R_{17}$  by bypassing some of the bias currents of differential pairs  $Q_{28}$ - $Q_{29}$  and  $Q_{30}$ - $Q_{31}$ . However, to keep the currents of transistors  $Q_{10}$  and  $Q_{11}$  constant and independent of the amount of dc shift  $V_S$ , the bypassed currents are added to the currents of  $R_{16}$  and  $R_{17}$ . Although  $V_C$  and  $\bar{V}_C$ , and hence  $V_S$ , are constant for our conventional VCO, this will not be the case once the ASC feedback is established.

In our implementation, the charging current  $I_C$  consists of two components: a coarse-tuning current and a fine-tuning current. This is to achieve the multiple center frequency requirement. These components are both generated by applying an internal bandgap voltage to an external resistor. Therefore,  $I_C$  is almost independent of process, temperature, and supply-voltage variations.

#### B. Relaxation VCO with ASC

Fig. 7 shows the circuit diagram of the ASC feedback VCO, which was designed to be added to the conventional VCO described above. In this circuit, transistors  $Q_{18}$  and  $Q_{19}$  and

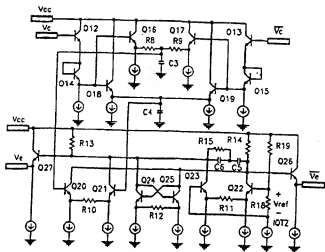


Fig. 7. Circuit diagram of the ASC feedback, which can be added to the oscillator of Fig. 4.

capacitor  $C_4$  extract the peak voltage of shifted versions of  $V_C$  and  $V_C$ .  $Q_{16}$ ,  $Q_{17}$ ,  $R_8$ ,  $R_9$ , and  $C_3$  extract the common-mode value of these voltages. The degenerated differential cell, consisting of  $Q_{20}$ ,  $Q_{21}$ , and  $R_{10}$ , converts the difference between the peak and common-mode voltages into a differential current. This current, which is representative of the oscillator swing, is subtracted from a reference current. The reference current is generated by applying the reference voltage  $V_{ref}$  to a matched degenerated differential cell composed of  $Q_{22}$ ,  $Q_{23}$ , and  $R_{11}$ . The net differential error current is converted back to voltage by resistors  $R_{13}$  and  $R_{14}$ .  $Q_{24}$ ,  $Q_{25}$ , and  $R_{12}$  are configured in a positive feedback to enhance the voltage gain of the error amplifier. The value of  $R_{12}$  was chosen to be slightly more than the sum of  $R_{13}$  and  $R_{14}$  and matched to them. This guarantees that the positive feedback never causes a latchup. The low-pass filter composed of  $C_5$ ,  $C_6$ , and  $R_{15}$  filters the error signal. This filter stabilizes the feedback loop and filters out the ripples introduced by the peak detector. When the ASC circuit is connected to the VCO of Fig. 6, the differential error signal  $V_e - V_r$  adjusts  $V_s$ , as explained earlier. It should be pointed out that this filter puts a constraint on the modulating frequency when the VCO is modulated by an external control voltage. For high modulating frequencies, the ASC loop fails to respond and the VCO gain drops to that of the conventional VCO. Therefore, the time constant of the ASC loop, set by the low-pass filter, must be chosen according to the maximum modulating frequency.

The reference voltage  $V_{ref}$  is used to compensate for temperature and process variations of the oscillator. In the present VCO, the frequency of oscillation tends to decrease with temperature due to parameters such as positive temperature coefficient of  $C_1$ , increase in the switching time of  $Q_1$  and  $Q_2$ , and temperature response of our ASC feedback circuit. This temperature dependency can be compensated by decreasing  $V_{ref}$ . The process variations can also be canceled out by trimming this voltage. Therefore,  $V_{ref}$  should have an appropriate combination of the following components: a component that has a negative temperature coefficient, a

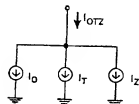


Fig. 8. Current  $I_{OTZ}$ .

component that can be trimmed, and a component with a fixed value. In our implementation,  $V_{ref}$  is generated by passing a current  $I_{OTZ}$  through the internal resistor  $R_{18}$  shown in Fig. 7. As shown in Fig. 8, the current  $I_{OTZ}$  is composed of three components. The first component  $I_O$  is generated by applying a bandgap voltage across an internal resistor. This part develops a fixed voltage drop across  $R_{18}$ , independent of process and temperature. The second component  $I_T$  is generated by a  $V_{BE}$  drop across an internal resistor and develops the voltage with the negative temperature coefficient. The third component  $I_Z$ , which can be trimmed with 6 bits of accuracy, generates a trimmed temperature-independent voltage. By on-wafer trimming of the current  $I_Z$ , the reference voltage  $V_{ref}$  is permanently adjusted such that a target frequency of oscillation is achieved at a predetermined amount of current  $I_s$ . The proper combination of  $I_O$  and  $I_T$  was first chosen based on simulations and was later adjusted based on measurement results. It should be pointed out that the ASC feedback removes the effect of  $T_d$  and consequently its large process-dependent effect on the oscillation frequency. Therefore, trimming at one frequency results in trimming the VCO from low frequencies (where  $T_d$  is negligible) up to high frequencies (where  $T_d$  is comparable to the period of oscillation).

#### IV. SIMULATION RESULTS

In this section, some of the simulation results for the VCO are provided to further demonstrate the effectiveness of the proposed ASC feedback. We will first compare the performance of the oscillators with and without ASC. Next, we will show how the ASC oscillator performs over process variations. Last, we will demonstrate how trimming can compensate process variations in the ASC oscillator.

The relaxation oscillator was simulated both with and without the ASC feedback (Figs. 6 and 7). This VCO was intended to be used in a phase-locked loop with a maximum loop bandwidth of few megahertz. The bandwidth of the ASC feedback loop was chosen to be 10 MHz. Therefore, the modulating frequency of the VCO is well within the frequency response of the ASC. The frequency and the peak value of the signal swing of the capacitor versus current are shown in Fig. 9. As can be seen, by applying the ASC, the linear frequency range of the VCO is extended significantly. The  $I$ - $F$  characteristic of the VCO without ASC starts to bend at about 200 MHz, while the  $I$ - $F$  characteristic of the ASC VCO goes up to about 700 MHz before starting to bend. The ASC feedback is also seen to increase the frequency of oscillation at the current level of 7 mA from 625 to 950 MHz. This

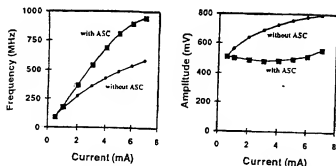


Fig. 9. Frequency and amplitude of oscillations with and without ASC.

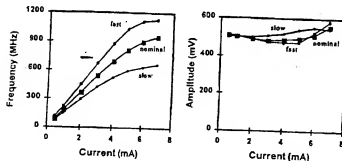


Fig. 10. Frequency and amplitude of oscillation of the ASC oscillator under process variation.

has been achieved by keeping the amplitude of oscillation fairly constant at about 500 mV (twice the reference voltage) and preventing it from increasing to 800 mV, as shown in Fig. 9.

Fig. 10 shows the characteristics of the ASC VCO simulated using the "nominal" model and two corner models "fast" and "slow," which cover the effect of process variations on the oscillator. In all three cases, the ASC feedback loop keeps the signal swing across the capacitor almost constant. However, because of different capacitance values in the three models (a variation of  $\pm 20\%$ ), the  $I$ - $F$  curves have different slopes: the largest slope for the "fast" case and the smallest slope for the "slow" case. The maximum frequency depends on the delay that is the smallest in the "fast" case (where we see the highest frequency) and the largest in the "slow" case (where we see the lowest frequency).

To have a VCO with an  $I$ - $F$  characteristic independent of process, the voltage  $V_{ref}$  is trimmed. As discussed in the previous section,  $V_{ref}$  is adjusted such that at a given current, the frequency of oscillation is that of the nominal process. In our simulation, the signal swing of the "fast" case must be increased to 600 mV, whereas the signal swing of the "slow" case must be decreased to 400 mV. Fig. 11 shows the simulation results of the ASC VCO after trimming at  $I_c = 1$  mA, corresponding to a frequency of 180 MHz. The  $I$ - $F$  characteristics overlap up to about 600 MHz. Above 600 MHz, the  $I$ - $F$  characteristic for the "slow" case starts to saturate toward its maximum value of 800 MHz. The frequency for the "fast" case overlaps the nominal frequency up to about 800 MHz. It should be pointed out that trimming does not affect the maximum limit

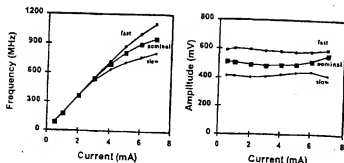


Fig. 11. Frequency and amplitude of oscillation of the ASC oscillator after trimming.

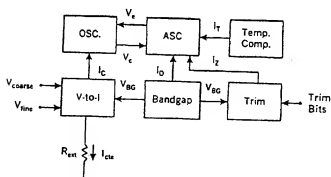


Fig. 12. Block diagram of the chip.

of the oscillation frequency, which is dictated by the delay  $T_d$ .

## V. IMPLEMENTATION

The ASC VCO was designed to have a frequency sweep range of 20–800 MHz [8]. The circuit was fabricated on a semicustom array in a bipolar process that offers NPN transistors with a cutoff frequency of 14 GHz and lateral PNP transistors with a cutoff frequency of 50 MHz. This process has two metal layers, poly resistors, and MOS and metal-to-metal capacitors.

Fig. 12 shows the block diagram of the implemented chip. A bandgap voltage is applied to an external resistor to generate a constant current  $I_{cle}$ . The voltage-to-current converter, which has a coarse and a fine tune input, generates the charging current  $I_c$  from  $I_{cle}$ . With the right combination of  $V_{coarse}$  and  $V_{fine}$ , shown in Fig. 12, the center frequency and tuning range of the VCO are set. The circuit schematics of the oscillator core and ASC blocks were shown in Figs. 6 and 7 and were discussed in detail in previous sections. The ASC block receives the currents  $I_o$ ,  $I_T$ , and  $I_Z$  from the bandgap, temperature compensation, and trim blocks, respectively. The trim block provides on-wafer trimming capability, which can be used to trim the center frequency of the VCO to within  $\pm 0.4\%$ . Having six trim bits allows successful trimming of the devices that experience a process variation of up to 50%. The micrograph of the implemented chip is shown in Fig. 13 with the various blocks highlighted.

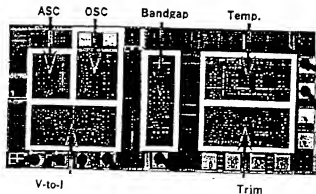
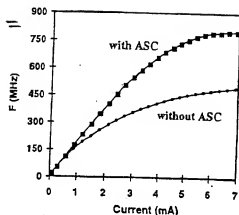


Fig. 13. Micrograph of the chip.

Fig. 14. Measured  $I$ - $F$  characteristic of the oscillator.

## VI. EXPERIMENTAL RESULTS

Fig. 14 shows the measured  $I$ - $F$  characteristic of the oscillator. With the ASC feedback inactive, the oscillator works up to only 500 MHz. A further increase in the current does not increase the frequency, as the voltage swing is also increased due to the effect of  $T_d$ . Once the ASC feedback is added, the frequency of oscillation reaches 800 MHz. Also, the linear range of the characteristic becomes considerably wider. These are in accordance with the theory and simulation results discussed earlier. It should be pointed out that as the current is reduced, the common-mode voltage of the capacitor terminals approaches the supply voltage and reduces the headroom for the capacitor voltage swing. This limits the low-frequency operation of the VCO to 20 MHz in both cases.

Fig. 15 shows the statistical data before and after trimming of more than 1000 IC's gathered from ten wafers fabricated in different process runs. As seen in Fig. 15(a), the frequency at a current of  $I_{c1}$  has a mean value of 351 MHz with a standard deviation of 87.4 MHz. Of these devices, only 5.5% experienced a process variation greater than 50% and were rejected. For the remaining 94.5%, on-wafer trimming was performed at the current level  $I_{c1}$ . The target frequency was 330 MHz, and the resulted standard deviation was 1.7 MHz. By switching the current to  $I_{c2}$ , the frequency had a mean value of 494.2 MHz and a standard deviation of only 3.7 MHz. The histograms after trimming are shown

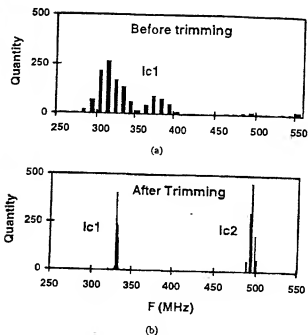


Fig. 15. Statistical data (a) before and (b) after trimming.

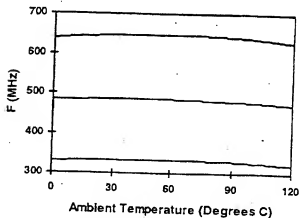


Fig. 16. Measured temperature behavior.

in Fig. 15(b). The small standard deviation at the second frequency is an indication that the  $I$ - $F$  characteristics of the trimmed IC's overlap regardless of the process variation. Therefore, current switching can be used to achieve a relatively accurate frequency switching. The process independence of the  $I$ - $F$  characteristic of the ASC VCO makes it attractive in autorate serial-digital video applications where a single VCO is required to operate in various frequency bands over a wide frequency range.

Fig. 16 illustrates the temperature measurements at three different operating frequencies of a plastic-packaged ASC VCO. A temperature coefficient better than  $-230$  ppm/ $^{\circ}\text{C}$  is achieved over a span of  $120^{\circ}\text{C}$ . It should be mentioned that as temperature rises,  $T_d$  increases and, consequently,  $f_{lim}$  drops. However, for frequencies below  $f_{lim}$ , the ASC feedback removes the effect of  $T_d$  and allows the temperature-compensation circuit to be effective even at an ambient temperature as high as  $120^{\circ}\text{C}$ . The plastic-packaged part was also

TABLE I  
TEMPERATURE MEASUREMENTS UNDER SUPPLY VARIATIONS

Supply Voltage (V)		Ambient Temperature (Degrees C)						
		0	20	40	60	80	100	120
4.75	F1 (MHz)	331	332	333	332	331	327	321
	F2 (MHz)	486	487	487	486	484	480	474
	F3 (MHz)	637	644	646	646	644	639	630
5.00	F1 (MHz)	330	332	332	332	331	327	321
	F2 (MHz)	484	485	486	485	482	478	472
	F3 (MHz)	637	644	646	646	644	638	628
5.25	F1 (MHz)	330	332	332	332	330	327	320
	F2 (MHz)	483	484	485	483	481	477	469
	F3 (MHz)	637	644	646	646	643	637	626

TABLE II  
POWER-SUPPLY REJECTION MEASUREMENTS

$f_n$ (MHz)	100	200	300	400	500	600
PSRR at $f_n$ (dB)	44	53	40	50	33	36
PSRR at $f_n$ offset from carrier (dB)	32	30	30	34	26	32

tested over supply variations of  $\pm 5\%$  across the 0–120°C temperature range. The results are summarized in Table I. For the stated change in the supply voltage, the frequency changes by only 0.6% at room temperature and changes not more than 1% over the entire temperature range.

The chip operates from a nominal power supply of 5 V and draws a total current of 18 mA.<sup>2</sup> The tuning range of the VCO is 30% of its center frequency. The phase noise of the oscillator measured at 370 MHz is  $-99$  dBc/Hz at 2-MHz offset. To measure the power-supply rejection, a 100-mV<sub>rms</sub> sinusoidal waveform was added to the supply voltage. This generates dominant tones at the applied frequency  $f_n$  and its folded frequency around the carrier. The power-supply rejection ratio (PSRR) at various applied frequencies is given in Table II. In this test, the carrier frequency was set to 580 MHz and had an output power of  $-4.3$  dBm. A rejection of better than almost 30 dB was observed. Table III summarizes the performance of the chip.

## VII. CONCLUSIONS

An ASC was presented for use with relaxation oscillators. It was shown that ASC both increases the linear frequency range and reduces the sensitivity of the oscillator to process and temperature variations. A collector-coupled relaxation oscillator was implemented in a 14-GHz bipolar process. While with ASC the frequency reaches 800 MHz, without

<sup>2</sup>A full-custom approach reduces the parasitic capacitances and requires less driving current. As a result, the higher limit of the operating frequency can be achieved with a smaller supply current.

TABLE III  
PERFORMANCE SUMMARY

Supply Voltage	5V
Supply Current	18mA
Frequency Range	20–800MHz
Tuning Range	30% of center frequency
Phase Noise (370MHz)	-99dBc/Hz@2MHz offset
PSRR	>26dB
Temperature Coefficient	-230ppm/°C over 120°C
Trim Accuracy	$\pm 0.4\%$ of center frequency
Trim Range	50% of center frequency
Technology	14GHz- $f_t$ bipolar, semi-custom

ASC it goes up to only 500 MHz. Statistical data were presented showing that by trimming the ASC VCO, the  $I$ - $F$  characteristic becomes independent of process variations over a wide frequency range. This means that only one external resistor and a  $V$ - $I$  converter are required to adjust the frequency in various bands over a wide range. These features make the ASC VCO attractive in autorate serial-digital video applications.

## ACKNOWLEDGMENT

The authors would like to thank J. Kendall, A. Cervin-Lawry, and A. Grzegorzczak for their help in modeling, fabrication, and test; and J. Francis and E. Ioszeff for their technical assistance.

## REFERENCES

- [1] B. Gilbert, "A versatile monolithic voltage-to-frequency converter," *IEEE J. Solid-State Circuits*, vol. SC-11, pp. 852–864, Dec. 1976.
- [2] M. Soyuer and J. D. Warnock, "Multigigahertz voltage-controlled oscillators in advanced silicon bipolar technology," *IEEE J. Solid-State Circuits*, vol. 27, pp. 668–670, Apr. 1992.
- [3] L. DeVito, "A versatile clock recovery architecture and monolithic implementation," in *Monolithic Phase-Locked Loops and Clock Recovery Circuits*, B. Razavi, Ed. New York: IEEE Press, 1996, pp. 405–420.
- [4] W. Mains, "Differential relaxation oscillator," *International Application Pub. WO 98/45944*, Oct. 1998.
- [5] S. Webster, E. Panthuser, K. Chen, J. Francis, E. Ioszeff, T. Rosati, I. Ridpath, and P. Moore, "A new chip set for proposed SMPTE standard SMPTE259M-Serial Digital Interface," *Soc. Motion Pictures Tele. Eng. J.*, pp. 777–785, Sept. 1993.

- [6] H. Shakiba and T. Sowlati, "Extended frequency range relaxation oscillator with improved linearity," U.S. Patent 2201 697, Apr. 1997.
- [7] L. DeVito, J. Newton, R. Croughwell, J. Bulzacchelli, and F. Benkley, "A 52MHz and 155MHz clock-recovery PLL," in *ISSCC Dig. Tech. Papers*, 1991, pp. 142-143.
- [8] T. Sowlati and H. Shakiba, "A 20-800MHz relaxation oscillator with automatic swing control," in *ISSCC Dig. Tech. Papers*, 1998, pp. 222-223.



Mohammad Hossein Shakiba (S'93-M'97) was born in Hamedan, Iran, in 1960. He received the B.Sc. (Hons.) and M.Sc. (Hons.) degrees from the Isfahan University of Technology, Iran, in 1985 and 1988, respectively, and the Ph.D. degree from the University of Toronto, Canada, in 1997, all in electrical engineering.

During 1986-1991, he was a Researcher and Lecturer in the Department of Electrical and Computer Engineering, Isfahan University of Technology. While pursuing the Ph.D. degree, he was a

Research Fellow in the Department of Electrical and Computer Engineering, University of Toronto. During this time, his research was focused on the area of high-speed data-communication systems. His doctoral work was related to the analog implementation of Viterbi detectors with emphasis on partial-response systems. He is currently interested in analog integrated-circuit design for wired and wireless data-communication systems. Since 1996, he has been with the R&D Video Group, Gennum Corp., Burlington, Ont., Canada, where he is a Senior IC Designer.



Tirdad Sowlati (S'94-M'97) was born in Tehran, Iran, in 1964. He received the B.A.Sc. (Hons.) and M.A.Sc. (Hons.) degrees in electrical engineering from Tehran Polytechnic University, Amir Kabir, Iran, in 1987 and 1989, respectively. He received the Ph.D. degree in electrical and computer engineering from the University of Toronto, Canada, in 1997.

He was a Design Engineer working on contracts with the Iranian Telecommunication Research Center in 1987 and the Research Center of Sharif

University during 1989-1990. He was the Microwave Lab Manager at Tehran Polytechnic University from 1989 to 1991 and a University Lecturer in communication circuits in 1990 and 1991. From 1992 to 1996, he worked on RFIC design at the Microelectronic Research Lab, University of Toronto. In 1996, he joined the Video Products R&D Group at Gennum Corp., Burlington, Ont., where he designed VCO's for data communication. He currently is a Senior Member of Research Staff with Philips Research, Briar Cliff Manor, NY, where he is working on power amplifiers for wireless communications. His research interests include RFIC design for wireless communications and high-speed circuit design for data communication.